Roles of paxillin family members in adhesion and ECM degradation coupling at invadosomes

Christos Petropoulos,[1,2,3] Christiane Oddou,[1,2,3] Anouk Emadali,[1,2] Edwige Hiriart-Bryant,[1,2,3] Cyril Boyault,[1,2,3] Eva Faurobert,[1,2,3] Scott Vande Pol,[4] Joo-ri Kim-Kaneyama,[5] Alexandra Kraut,[6,7,8] Yohann Coute,[6,7,8] Marc Block,[1,2,3] Corinne Albiges-Rizo,[1,2,3]* and Olivier Destaing[1,2,3]*

[1]Institut Albert Bonniot, Institut National de la Santé et de la Recherche Médicale U823, 38042 Grenoble, France
[2]Université Grenoble Alpes, 38400 Saint-Martin-d'Hères, France
[3]Equipe de Recherche Labellisée, Centre National de la Recherche Scientifique 5284, 38042 Grenoble, France
[4]Department of Pathology, University of Virginia, Charlottesville, VA 22908
[5]Department of Biochemistry, Showa University School of Medicine, Tokyo 142-8555, Japan
[6]Institut de Recherche en Technologies et Sciences pour le Vivant-Biologie à Grande Échelle, Université Grenoble Alpes, 38000 Grenoble, France
[7]Commissariat à l'Énergie Atomique et aux Énergies Alternatives, Institut de Recherche en Technologies et Sciences pour le Vivant-Biologie à Grande Échelle, 38000 Grenoble, France
[8]Institut National de la Santé et de la Recherche Médicale, Laboratoire Biologie à Grande Échelle, 38000 Grenoble, France

Invadosomes are acto-adhesive structures able to both bind the extracellular matrix (ECM) and digest it. Paxillin family members—paxillin, Hic-5, and leupaxin—are implicated in mechanosensing and turnover of adhesion sites, but the contribution of each paxillin family protein to invadosome activities is unclear. We use genetic approaches to show that paxillin and Hic-5 have both redundant and distinctive functions in invadosome formation. The essential function of paxillin-like activity is based on the coordinated activity of LD motifs and LIM domains, which support invadosome assembly and morphology, respectively. However, paxillin preferentially regulates invadosome assembly, whereas Hic-5 regulates the coupling between ECM degradation and acto-adhesive functions. Mass spectrometry analysis revealed new partners that are important for paxillin and Hic-5 specificities: paxillin regulates the acto-adhesive machinery through janus kinase 1 (JAK1), whereas Hic-5 controls ECM degradation via IQGAP1. Integrating the redundancy and specificities of paxillin and Hic-5 in a functional complex provides insights into the coupling between the acto-adhesive and ECM-degradative machineries in invadosomes.

Introduction

Invadosome are acto-adhesive structures composed of a dense F-actin core surrounded by a ring of adhesion molecules, particularly β1 and β3 integrins (Destaing et al., 2010; Schmidt et al., 2011). All models of invadosomes, including invadopodia and podosomes, have been implicated in cellular invasion (Linder, 2007, 2009; Albiges-Rizo et al., 2009; Destaing et al., 2011; Murphy and Courtneidge, 2011; Saltel et al., 2011; Boateng and Huttenlocher, 2012). Expression of the constitutively active mutant of c-Src (SrcY527F) induces isolated invadosomes that can autoassemble into circular metastructures called invadosome rings (Tarone et al., 1985; Chen, 1989; Destaing et al., 2003, 2010; Albiges-Rizo et al., 2009). Invadosomes are characterized by an antagonist behavior, combining intense actin polymerization and adhesion to the ECM with local degradation caused by the delivery of metalloproteases such as membrane type 1 metalloproteinase (MT1-MMP; Poincloux et al., 2009).

The activation of the adhesion machinery leads to invadosome stabilization and consequently improves its ability to digest the ECM (Branch et al., 2012; Sharma et al., 2013). One of the mechanisms involved in degradation is the control of local delivery of MT1-MMP at the plasma membrane by the exocyst complex, through its recruitment by IQGAP1, a CDC42 effector (Sakurai-Yageta et al., 2008; Branch et al., 2012). However, little is known about the molecular basis of the coupling between acto-adhesion and ECM degradation.

Paxillin family members are molecular adaptors known to interact with integrins and regulate the dynamics of adhesion sites. In mammals, the paxillin family is represented by three members: paxillin, Hic-5, and leupaxin. Little is known about the relationship between paxillin family members and their respective roles in invadosomes. Structurally, all members of the paxillin family are characterized by two domains involved in protein–protein interactions. The N-terminus part is composed

of five LD motifs (consensus LD*XLLXX*L) that form amphipathic α-helices that are important for the binding of multiple adhesive regulators (Sattler et al., 2000; Tumbarello et al., 2002). LD1 and LD2/4 motifs are the binding sites for vinculin, and LD2 and LD4 interact with focal adhesion kinase (FAK; Turner and Miller, 1994; Brown et al., 1996). Although the interactors of some LD motifs are well characterized, the partners of the LD3 and LD5 motifs of paxillin are not well known. The C-terminal half of paxillin is composed of four LIM domains (LIM1–LIM4) known to form double zinc-finger motifs (Pérez-Alvarado et al., 1994; Schmeichel and Beckerle, 1994). The LIM2 and LIM3 domains are essential for targeting paxillin to focal adhesions (Brown et al., 1996), and all LIM domains are essential for the recruitment of paxillin to stress fibers under tension (Smith et al., 2013; Watanabe-Nakayama et al., 2013).

In invadosomes, live imaging monitoring in osteoclasts has shown that the recruitment of paxillin is an early event in the formation of these acto-adhesive structures (Luxenburg et al., 2012), but it also regulates their disassembly when phosphorylated by Src and FAK (Brown and Turner, 2004; Webb et al., 2004; Zaidel-Bar et al., 2007; Badowski et al., 2008; Zou et al., 2012). Whereas the role of paxillin regulates adhesion site dynamics, Hic-5 has been implicated in the activation of ECM degradation. Hic-5 up-regulation induced by TGF-β in epithelial cells promotes elevated ECM proteolysis through invadosome formation (Pignatelli et al., 2012).

We addressed the question of whether the coupling between the acto-adhesive activity and ECM degradation activity of invadosomes might be regulated by the cooperation between paxillin family members. Genetic approaches were used to decipher the family members' respective functions in invadosomes. Our results show that paxillin and Hic-5 have both redundant and specific functions in invadosome formation. Structure–function studies revealed that paxillin LIM-containing domains, in contrast to focal adhesions, were not important in localizing paxillin in invadosomes but were essential in regulating their morphology, and each LD motif was essential for inducing their formation. In addition to their redundant functions, paxillin preferentially regulates invadosome assembly, and Hic-5 appears to be more important for invadosome disorganization and the coupling between ECM degradation and acto-adhesive functions. Mass spectrometry analysis of the paxillin interactome identified new binding partners of paxillin as being implicated in regulation of the acto-adhesive machinery (janus kinase 1 [JAK1]) and ECM degradation (IQGAP1). Considering both their redundancy and their specificities, our study reveals that paxillin and Hic-5 form a functional complex important for the coupling between the acto-adhesive and ECM-degradation machineries in invadosomes.

Results

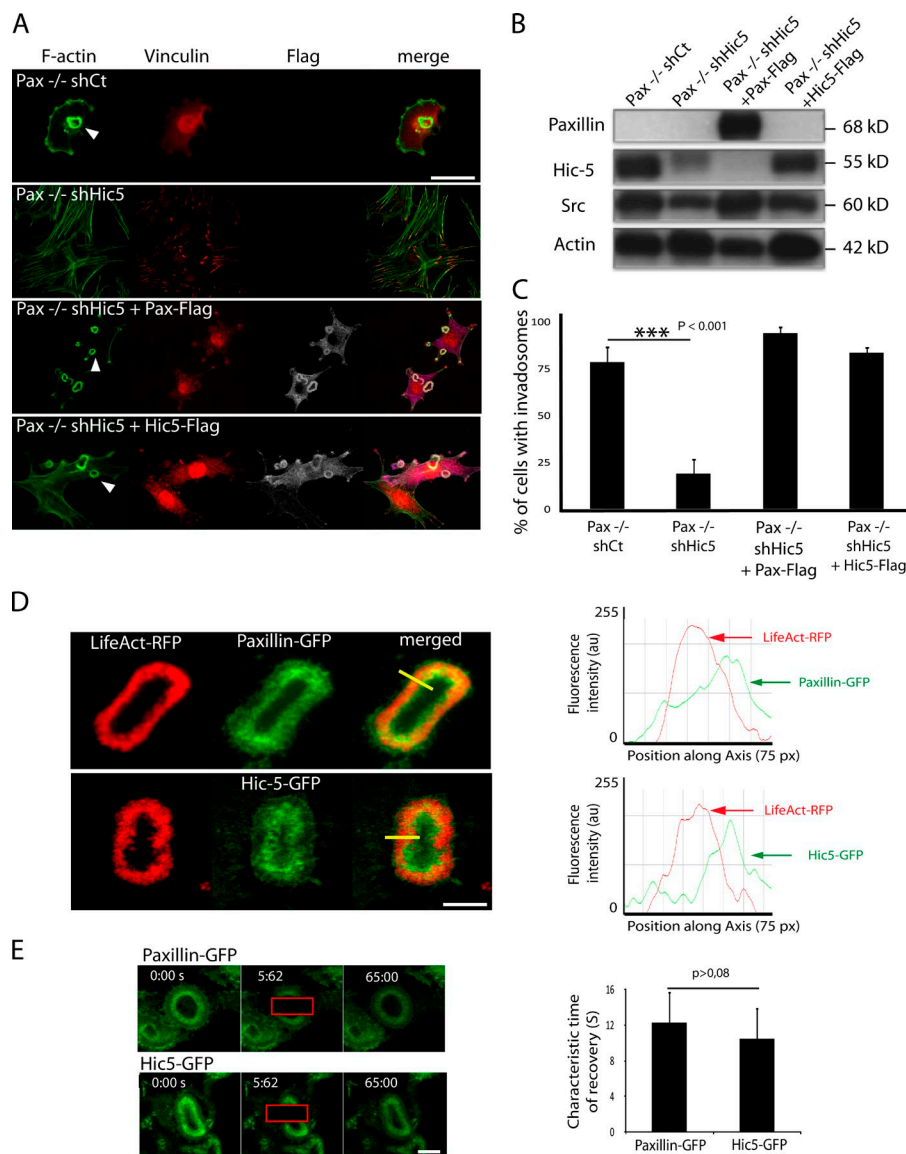### Functional redundancy of paxillin and Hic-5 in the formation of invadosomes

Despite the fact that loss-of-function strategies can reveal the function of a protein role in a cellular process, it is not so clear when related proteins of the same family exert similar activities. Therefore, we considered the functions of all paxillin family members (paxillin, Hic-5, and leupaxin) in the regulation of the complex structure as invadosomes. The preliminary results showed that invadosomes formed in pax$^{-/-}$ cells after expression of the constitutively active form of the proto-oncogene c-Src (SrcY527F; Fig. 1, A and C). The fact that pax$^{-/-}$ cells expressing SrcY527F could form isolated and ring-shaped invadosomes (Fig. 1, A–C) can be explained by either a compensatory mechanism mediated by Hic-5 and leupaxin or by both proteins having an essential function in invadosome formation. To discriminate between the potentially redundant functions of each protein, compensatory mechanisms, and essential functions of leupaxin/Hic-5 in these structures, invadosomes were analyzed in pax$^{-/-}$ cells expressing SrcY527F treated with nonspecific shRNA or shRNA targeting Hic-5. Hic-5 silencing dramatically reduced the formation of both isolated and ring-shaped invadosomes in the pax$^{-/-}$ genetic background (Fig. 1, A–C). Thus, it appeared that the remaining expression of leupaxin in SrcY527F pax$^{-/-}$ shHic-5 cells could not compensate for the loss of paxillin and Hic-5 in the regulation of invadosome formation. The low level of remaining Hic-5 in SrcY527F pax$^{-/-}$ shHic-5 cells (Fig. 1 B) was not sufficient to maintain invadosome assembly (Fig. 1, A and C). Other adhesive structures, such as focal adhesions, were still present, indicating that invadosomes were more sensitive to paxillin and Hic-5 depletion (Fig. 1 A). These data suggest that Hic-5 is an essential protein for invadosome formation. To confirm this hypothesis, reverse genetics was performed by reintroducing either paxillin wild-type (pax-WT)-Flag or Hic-5-WT-Flag in these SrcY527F pax$^{-/-}$ shHic-5 cells. Surprisingly, both paxillin and Hic-5 reexpression perfectly restored invadosome formation (Fig. 1, A–C). Therefore, Hic-5 is not the only central protein for invadosome formation; paxillin and Hic-5 have shared functions in the formation of these acto-adhesive structures. Thus, it appears that invadosomes are highly dependent on paxillin-like activity (paxillin and/or Hic-5). It is also important to note that the reexpression of paxillin-WT-Flag largely increased the efficiency of Hic-5 silencing in SrcY527F pax$^{-/-}$ shHic-5 cells (Fig. 1 B), which shows that paxillin reexpression directly affected Hic-5 stability in this context. This finding suggests that cells can sense and maintain paxillin-like activity (paxillin or Hic-5). Integrating genetic and reverse-genetic data suggests that the balance between paxillin and Hic-5 functions is important for invadosome formation.

To further examine the redundancy of paxillin and Hic-5 functions, their localization and dynamics were investigated in invadosomes. GFP-tagged versions of paxillin and Hic-5-WT forms were used to localize each protein in invadosome rings of mouse embryonic fibroblast (MEF)–SrcY527F cells. Both proteins were localized across the invadosome ring (Fig. 1 D). More specifically, GFP-paxillin and GFP-Hic-5 were localized in two different regions of the invadosome ring, as shown by fluorescence intensity scans along the ring axis (Fig. 1 D): (a) as a thin line surrounding the invadosome ring and (b) as an increasing gradient from the outer rim to the inner rim of the ring (Fig. 1 D). Paxillin and Hic-5 did not present different molecular mobility, whereas the mean characteristic time of recovery of GFP-tagged paxillin and Hic-5, as measured by FRAP, was not significantly different (Fig. 1 E). Thus, the functional redundancy of paxillin and Hic-5 in invadosome formation is supported by their identical localization and mobility.

Cooperation of paxillin LD motifs and LIM domains in invadosome formation and morphology

The absence of isolated invadosomes or invadosome rings in SrcY527F-pax$^{-/-}$ shHic-5 cells led us to use this cellular model

Figure 1. **Functional redundancy of paxillin and Hic-5 in invadosome formation.** (A) Paxillin depletion in MEF-SrcY527 cells does not affect invadosome formation. The reexpression of either pax-WT-Flag or Hic-5-WT-Flag reinduces the formation of invadosomes easily recognized by their ring shape (arrowheads). (B) Western blot analysis of pax$^{-/-}$ cells expressing or not expressing Hic-5 or pax-WT-Flag. shRNA treatment efficiently decreased the endogenous protein levels of Hic-5, whereas expression of pax-WT-Flag reinforced the effects of Hic-5 silencing. (C) Quantification of the percentage of cells forming invadosomes in MEF-SrcY527F pax$^{-/-}$ cells rescued or not rescued with Hic-5 or pax-WT-Flag shows the redundancy of both proteins ($n = 4$; 500 cells per condition). ***, $P < 0.001$. (D) Representative analysis of the fluorescence intensity profile of paxillin-GFP or Hic-5-GFP and LifeAct-RFP over the yellow lines going through the invadosome revealed the same distribution of both proteins as a crescent-shaped gradient from the inner to the outer rims ($n = 4$). au, arbitrary unit. (E) FRAP experiments ($n = 3$) performed on MEF-SrcY527F cells expressing either paxillin-GFP or Hic-5-GFP revealed that both proteins presented the same mobility in invadosomes. Red rectangles show where the photobleaching is induced. All graphs presented as means ± SD. Differences with a probability level $P < 0.05$ were considered significant in one-way ANOVA. Bars: (A) 10 µm; (D) 2 µm; (E) 4 µm.

to explore the molecular basis of the paxillin-like activity in invadosome regulation. Based on paxillin's and Hic-5's redundancy and structural homology, truncated mutants of paxillin were reexpressed to determine for the first time the functions of the LD and LIM domains in invadosomes. Because LIM-containing proteins are known to be important for focal adhesion maturation (Brown et al., 1996; Smith et al., 2013), we examined whether paxillin's LIM domains were necessary to induce invadosome formation. To address this question, the number of invadosomes was quantified in SrcY527F pax$^{-/-}$ shHic-5 fibroblasts rescued by pax-WT-Flag or pax-ΔLIM-Flag (deleted for the four LIM domains; Fig. 2 A). Surprisingly, expression of pax-ΔLIM-Flag mutant in SrcY527F-pax$^{-/-}$ shHic-5 cells efficiently rescued invadosome formation (Fig. 2, B and C). However, these invadosome rings are larger (Fig. 2 B) while presenting a higher surface area and a larger perimeter, whereas their thickness is not changed (Fig. S1 A). Cells transfected with pax-ΔLIM presented invadosomes displaying a slow turnover compared with SrcY527F-pax$^{-/-}$ shHic-5 cells rescued with pax-WT (Fig. S1 B). Moreover, this decrease in invadosome dynamics was associated with a significant reduction of the net flux of actin

(Fig. S1 C). Finally, these larger invadosomes formed in cells rescued with pax-ΔLIM presented a significant decrease in matrix degradation (Figs. 2 D and S2 A), showing that paxillin's LIM domains are essential for invadosomes' proteolytic activity. In contrast to their function in focal adhesion, LIM domains are not essential for paxillin targeting in invadosomes but are important in regulating their acto-adhesive properties (assembly, morphology, and dynamics) and their degradative function.

Because the N-terminal part of paxillin was sufficient to restore invadosome formation, the contribution of each paxillin LD motif (LD1–LD5) was further explored in the regulation of invadosome formation. For that purpose, multiple pax-Flag mutants depleted for each LD sequence (ΔLD1–ΔLD5) were expressed in SrcY527F pax$^{-/-}$ shHic-5 cells (Fig. 2, A and E). Surprisingly, each LD-depleted paxillin mutant showed poorly rescued formation of invadosome rings. Isolated invadosomes and a limited number of semicircular structures still formed but did so to a lesser extent than in SrcY527F pax$^{-/-}$ shHic-5 cells that reexpressed the pax-WT-Flag form. All LD motifs are important in invadosome ring assembly (Fig. 2, E and F), which suggests that cooperativity between LD motifs is necessary for
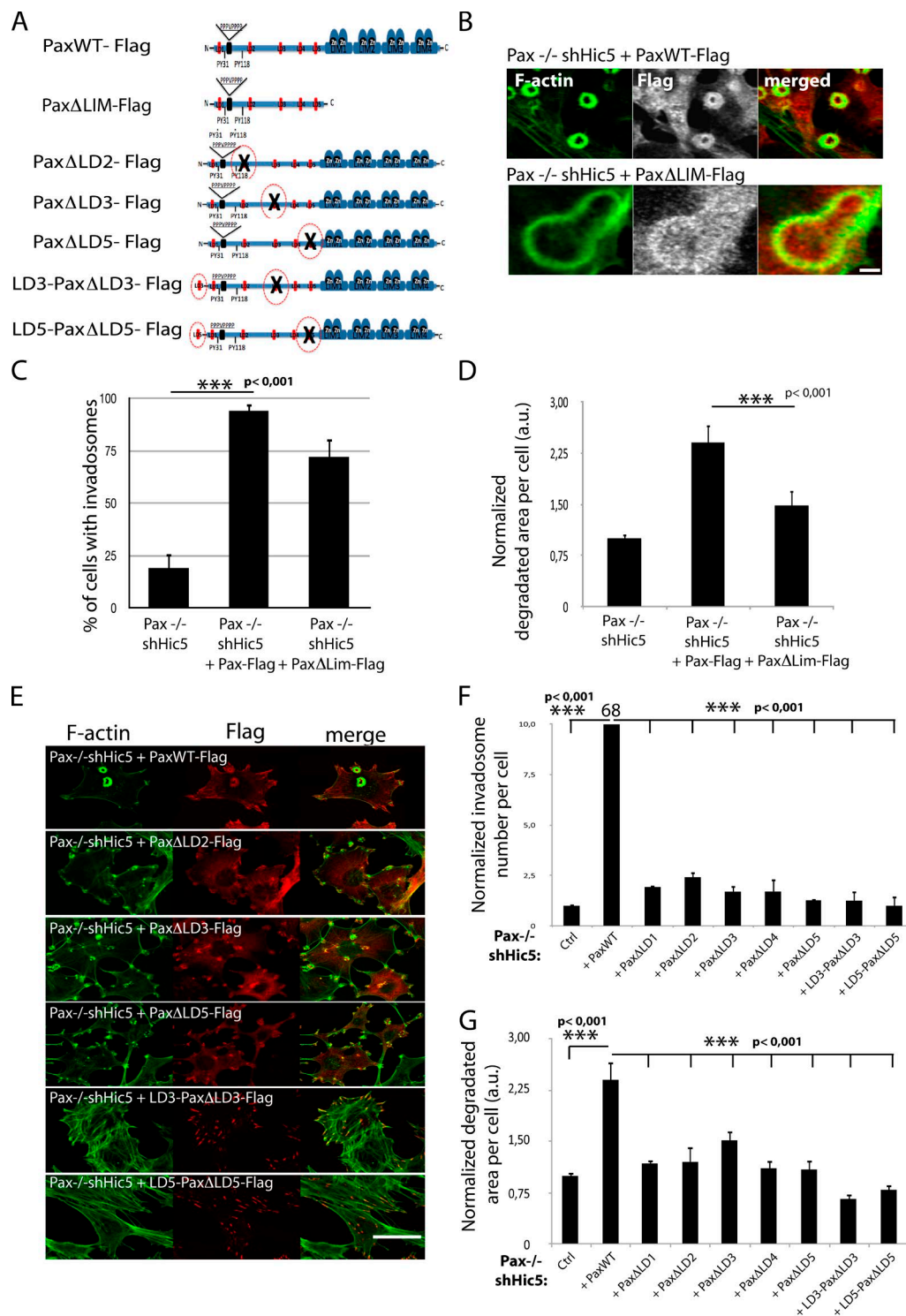
Figure 2. **Structure–function studies revealed the properties of LIM and LD domains in invadosomes.** (A) Schematic representation of the pax-Flag-WT and pax-Flag mutants missing the LIM domains and pax-Flag mutants deleted for the LD1, LD2, LD3, LD4, or LD5 motifs used for structure–function studies. (B) MEF-SrcY527F pax$^{-/-}$ shHic-5 cells expressing pax-Flag-WT induced very compacted invadosomes, whereas pax-ΔLIM-Flag expression resulted in large rings. (C) Quantification of the percentage of cells forming invadosomes revealed that pax-ΔLIM-Flag mutants rescued invadosome formation as well as pax-Flag-WT ($n = 3$; 300 cells counted per condition). (D) Quantification of the normalized degraded area of fluorescent gelatin per cell revealed that expression of the pax-ΔLIM-Flag mutant poorly restored ECM degradation in comparison to pax-Flag-WT ($n = 3$; 200 cells counted per condition). au, arbitrary unit. (E) Immunofluorescence experiments showing the absence of invadosome rings caused by the absence of LD1, LD2, LD3, LD4, or LD5 motifs, whereas some isolated invadosomes were still visible. The expression of either pax-LD3_ΔLD3-Flag or pax-LD5_ΔLD5-Flag completely abolished the formation of isolated invadosome rings. (F) Quantification of the percentage of cells forming invadosomes showed that deletion of each LD poorly restored invadosome ring formation in comparison to pax-WT-Flag ($n = 3$; 300 cells counted per condition). (G) Quantification of the normalized degraded area of fluorescent gelatin per cell shows that the decrease of invadosome formation induced by each mutant was associated with low ECM degradation. ***, $P < 0.001$. All graphs presented as means ± SD. Differences with a probability level $P < 0.05$ were considered significant in one-way ANOVA. Bars: (B) 8 µm; (E) 20 µm.

the proper function of paxillin in invadosome formation. Moreover, decreased ring formation in the cells rescued with the pax-ΔLD mutants was directly associated with low levels of ECM proteolytic activity (Figs. 2 G and S2 A). Supplementing what is known about paxillin functions in focal adhesions, we showed that the poorly characterized LD3 and LD5 domains were essential in the restoration of invadosome ring formation (Fig. 2, E and F). Therefore, we focused our work on these motifs by investigating whether paxillin LD3/LD5 function in ring assembly was dependent on their ability to recruit and coordinate multiple partners. To test this hypothesis, the LD3 and LD5 motifs were reintroduced at the N-terminus of the pax-ΔLD3-Flag and pax-ΔLD5-Flag mutants, respectively (Fig. 2 A). The reexpression of these new mutants (pax-LD3_ΔLD3-Flag and pax-LD5_ΔLD5-Flag) did not restore the formation of invadosome ring formation; rather, it blocked the formation of the rare isolated invadosomes present in cells that reexpressed pax-ΔLD3-Flag and pax-ΔLD5-Flag mutants (Fig. 2, E and F). Similarly, cells rescued by pax-LD3_ΔLD3-Flag and pax-LD5_ΔLD5-Flag displayed decreased ECM degradation activity (Figs. 2 G and S2 A). These data show that the position of LD domains is a key element in cooperativity, which is likely dictated by a specific tertiary structure induced by different LD domains. Collectively, our results reveal that paxillin is not a linear adaptor protein in which each LD separately recruits interacting proteins; rather, its LD motifs cooperate, thereby facilitating paxillin's proper function.

In addition to their redundancy, paxillin and Hic-5 have specific functions in invadosomes

Reverse genetics revealed that paxillin and Hic-5 have redundant functions. However, their specific functions in invadosome assembly and activity might be masked by compensatory mechanisms and cell adaptation. To explore the specific functions of paxillin and Hic-5 in invadosomes, a silencing strategy that individually or simultaneously targeted paxillin and Hic-5 was used to induce their rapid depletion in MEF-SrcY527F cells. siRNA treatment was efficient, leading to 90% and 85% decreases in paxillin and Hic-5 protein levels, respectively (Fig. 3 A). Notably, paxillin silencing induced a significant increase in Hic-5 protein levels, whereas the targeting of Hic-5 by siRNA resulted in increased protein levels of paxillin (Fig. 3 A, left). This compensatory mechanism between paxillin and Hic-5 occurred at the protein level and not at the mRNA level (Fig. 3 A, right). This confirmed that the reexpression of pax-WT-Flag largely increased the efficiency of Hic-5 silencing in SrcY527F pax⁻/⁻ shHic-5 cells (Fig. 1 B). Thus, it appears that cells can adapt the functions of paxillin–Hic-5 balance by modulating the stability of each of these proteins.

Next, we assessed whether invadosome dynamics might be affected by the depletion of one of the paxillin members. Notably, the rapid depletion of paxillin led to a decrease in invadosome rosette formation, which is associated with an increase in rosette thickness and suggests a perturbation in the assembly–disassembly rate of this structure (Fig. 3 B). Surprisingly, Hic-5 silencing significantly increased the mean number of invadosome rings per cell (Fig. 3 B), correlating with an increase in paxillin expression (Fig. 3 A). Finally, the simultaneous paxillin and Hic-5 silencing was characterized by small invadosome aggregates and a larger decrease in invadosome formation than paxillin depletion alone (Fig. 3 B), confirming our genetic approach (Fig. 1, A and C). Altogether, our results show that

although paxillin and Hic-5 have redundant functions, paxillin represents a key molecule that is necessary for ring assembly.

Then the precise function of paxillin and Hic-5 in the acto-adhesive functions of invadosomes was explored. Live imaging revealed that MEF-SrcY527F cells expressing Life-Act-GFP silenced for paxillin exhibited very thick rings that persisted over time (Fig. 3 F, red arrowheads) compared with rings in control cells (Fig. 3 F, multicolored arrowheads). The stabilization of invadosomes induced by paxillin depletion was not associated with a change in the net flux of GFP-actin, as measured by FRAP (Fig. 3 E). Instead, Hic-5–silenced cells formed invadosome rings with no obvious change in their dynamics compared with control cells (Fig. 3 F). The subsequent question was to determine whether the depletion of paxillin or Hic-5 might affect the degradative activity of invadosomes.

Paxillin silencing was associated with a decrease in ECM-degradation activity, as revealed by the inefficiency in fluorescent ECM layer digestion (Figs. 3 D and S2 B), which was likely caused by reduced invadosome numbers (Fig. 3 C). Surprisingly, Hic-5 silencing strongly reduced the ECM-degradation activity (Fig. 3 D) despite the elevated invadosome numbers (Fig. 3 C). No supplemental effects were observed in ECM degradation when both paxillin and Hic-5 were depleted simultaneously (Figs. 3 D and S2 B). In conclusion, paxillin and Hic-5 have a complementary function in a fully active invadosome, whereas paxillin preferentially activates the adhesive activity of invadosome, and Hic-5 is more specialized in the regulation of the ECM degradation of invadosomes.

Identification of specific interactors of paxillin and Hic-5 in MEFSrcY527F

To explore the molecular basis of their respective functional specificity, partners of paxillin and Hic-5 were identified in the context of cells expressing SrcY527F. For that purpose, pax-WT-Flag and Hic-5-WT-Flag were expressed in SrcY527F-expressing cells depleted of the respective endogenous proteins (Fig. 4 A). The coimmunoprecipitated binding partners of each Flag-tagged protein were identified through mass spectrometry analysis. A Venn diagram analysis showed that paxillin and Hic-5 shared 10 common proteins; 41 specific binding partners were copurified for pax-WT-Flag; and 23 specific interactors were determined for Hic-5-WT-Flag (Fig. 4 B and Table S1). Well-known paxillin interactors such as GIT1, GIT2, and tyrosine phosphatase MPTP-PEST were sorted out. A significant enrichment of actin-nucleating proteins and the actin-depolymerization factor cofilin were also found for paxillin (Fig. 4 B and Table S2). It appeared that paxillin interacted with numerous signaling molecules and cytoskeleton regulators. Moreover, only paxillin was able to bind cytoskeletal motors such as myo1D/E, myo5, and myo6 and a novel regulator of cell contractility, JAK1. Among the numerous Hic-5 interactors, it is particularly interesting to note the specific recruitment of IQGAP1, a CDC42 effector.

To investigate the poorly known specific interactors of LD3 and LD5 motifs, a semiquantitative mass spectrometry approach was applied on complexes copurified with pax-WT-Flag, pax-ΔLD3-Flag, pax-ΔLD5-Flag, pax-LD3_ΔLD3-Flag, or pax-LD5_ΔLD5-Flag. Numerous interactors of pax-WT-Flag, such as Arp2 and 3, JAK1 (interaction regulated by both LD3 and LD5), and GIT1, were either absent or exhibited less binding (as revealed by a decrease in the number of peptides specific to these proteins and coimmunoprecipitated with the
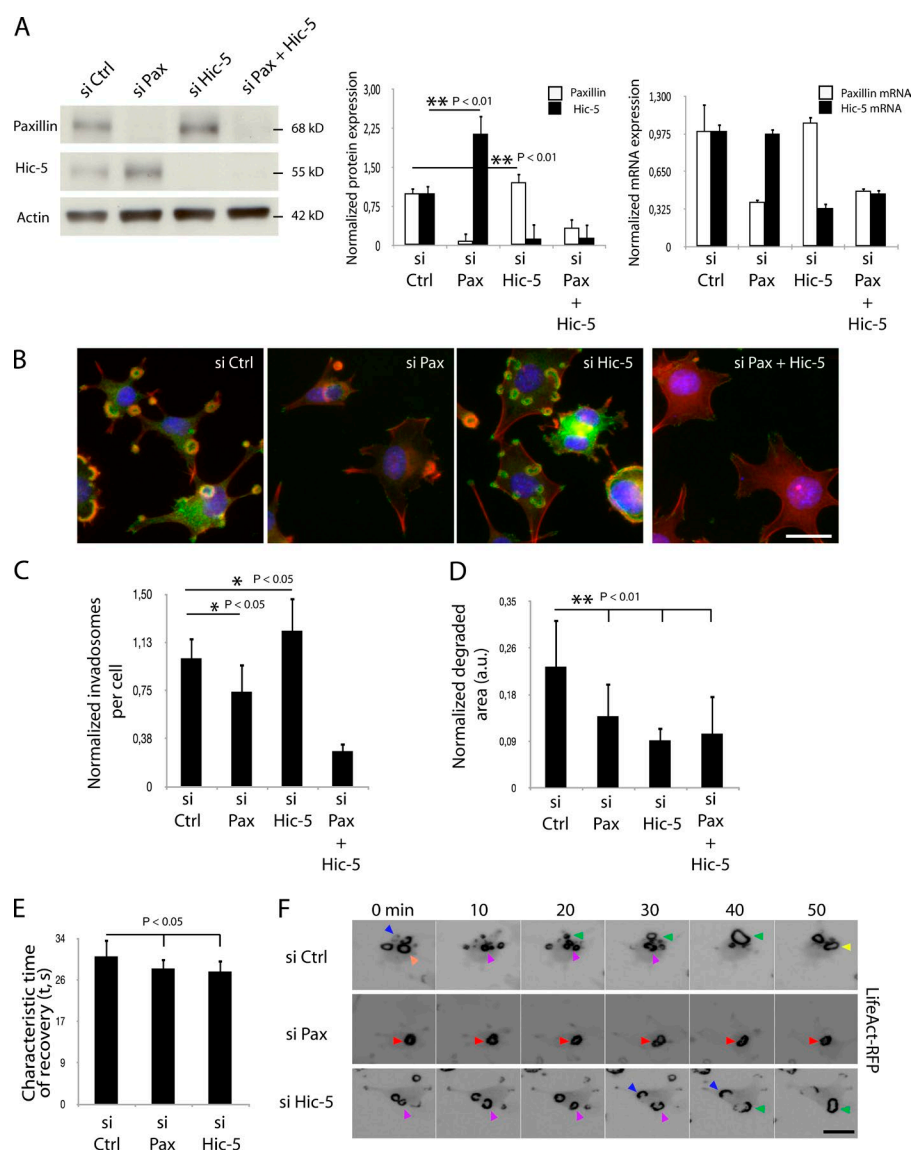
Figure 3. **Paxillin- and Hic-5–specific functions in invadosome formation and activity.** (A) Representative Western blot of cell lysates from MEF-SrcY527F cells treated with control, paxillin, Hic-5, or both paxillin and Hic-5 siRNA (left). Quantification of paxillin and Hic-5 revealed that the acute depletion of each protein led to an adaptation response by increasing the protein levels of its related protein ($n = 5$; middle). Quantification by quantitative real-time PCR showed that the siRNA treatment affected only the targeted mRNA without affecting the counteract protein mRNA ($n = 3$; right). (B) MEF-SrcY527F cells treated with control, paxillin, Hic-5, or paxillin and Hic-5 siRNA were spread on fibronectin-coated glass coverslips and stained with anti-paxillin antibody (green) and F-actin (red). (C) Quantification of the normalized number of invadosome rings per cell revealed that paxillin silencing decreased the number of invadosome rings per cell, whereas silencing of Hic-5 significantly increased it ($n = 3$, 300 cells counted per condition). (D) Quantification of the mean degradation area per cell revealed that all siRNA treatments decreased the degradation activity compared with the control ($n = 3$; 200 cells counted per condition). **, $P < 0.01$. (E) Quantification of the GFP-actin characteristic time of recovery showed that the depletion of both paxillin and Hic-5 did not affect actin mobility in invadosomes ($n = 3$). (F) Representative images extracted from a time series of MEF-SrcY527F cells stably expressing LifeAct-GFP and transfected with specific siRNAs (control, paxillin, or Hic-5). Paxillin depletion resulted in very thick and hyperstable invadosome rings, whereas Hic-5-knockdown cells exhibited normal dynamics, as in the control siRNA-treated cells. All graphs presented as means ± SD. Differences with a probability level $P < 0.05$ were considered significant in one-way ANOVA. Bars: (A) 6 µm; (F) 15 µm.

indicated flag mutants; Table S3) compared with the pax-WT-Flag form. Thus, the repositioning of the LD3 and LD5 domains at the N-terminal part of the pax-ΔLD3-Flag or the pax-ΔLD5-Flag did not restore the binding of specific pax-WT-Flag interactors but even decreased the number of other paxillin interactors (Table S3). Therefore, it appears that the correct positioning of LD domains is a key element to control paxillin interactions, which most likely occur on a characteristic tertiary structure. Moreover, this approach allowed us to determine the interactors of pax-WT-Flag dependent on the presence of the poorly known LD3 and LD5 domains (Fig. S3). Because

recent studies have highlighted the importance of JAK1 in tumor cell invasion (Sanz-Moreno et al., 2011; Albrengues et al., 2014; Orgaz et al., 2014) and the role of IQGAP1 in matrix remodeling (Sakurai-Yageta et al., 2008), we focused on these binding partners.

JAK1 is associated with the acto-adhesive function of paxillin

JAK1 as a potential new paxillin interactor was particularly interesting, because this kinase has recently been associated with tumor invasion and contractile machinery (Sanz-Moreno et al.,
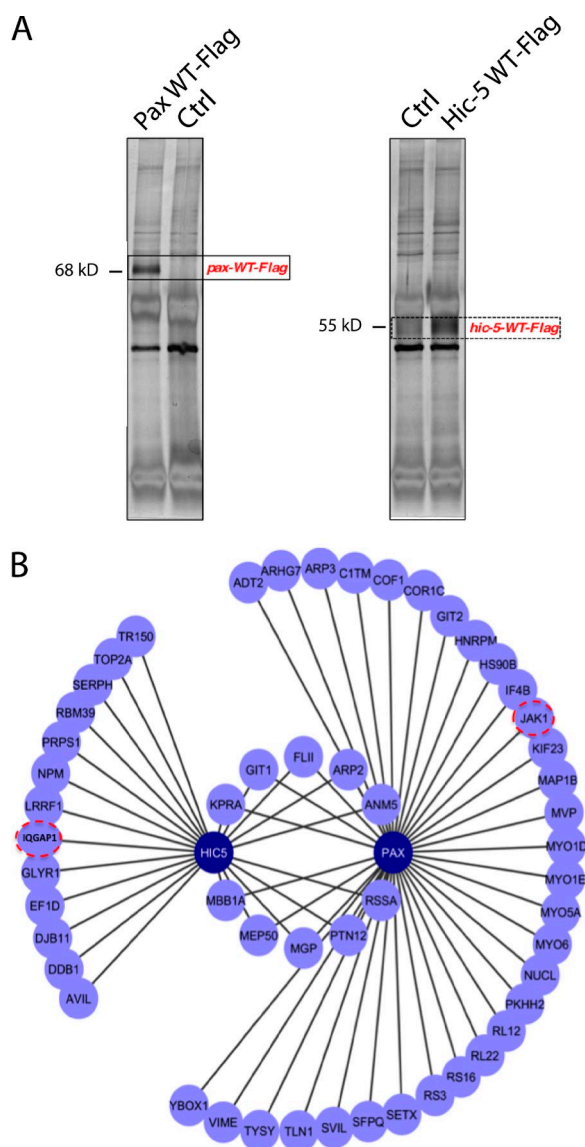
Figure 4. **Specific paxillin and Hic-5 interactors.** (A) SDS-PAGE (10% gel) and silver staining analysis of paxillin and Hic-5 binding partners copurified with either pax-WT-Flag or Hic-5-WT-Flag. The control condition corresponds to cell lysates of paxillin- and Hic5-deficient cells (pax⁻/⁻ and hic⁻/⁻ cells) with nonspecific IgG but with the same isotype as anti-Flag M2. (B) Cytoscape visualization of the specific and shared interactors between paxillin and Hic-5 (dark blue). In these cellular and purification conditions, paxillin interacts with numerous acto-adhesive regulators and the newly contractile regulator JAK1. Hic-5 interacts with less acto-adhesive regulators but can bind specifically to exocyst regulator IQGAP1.
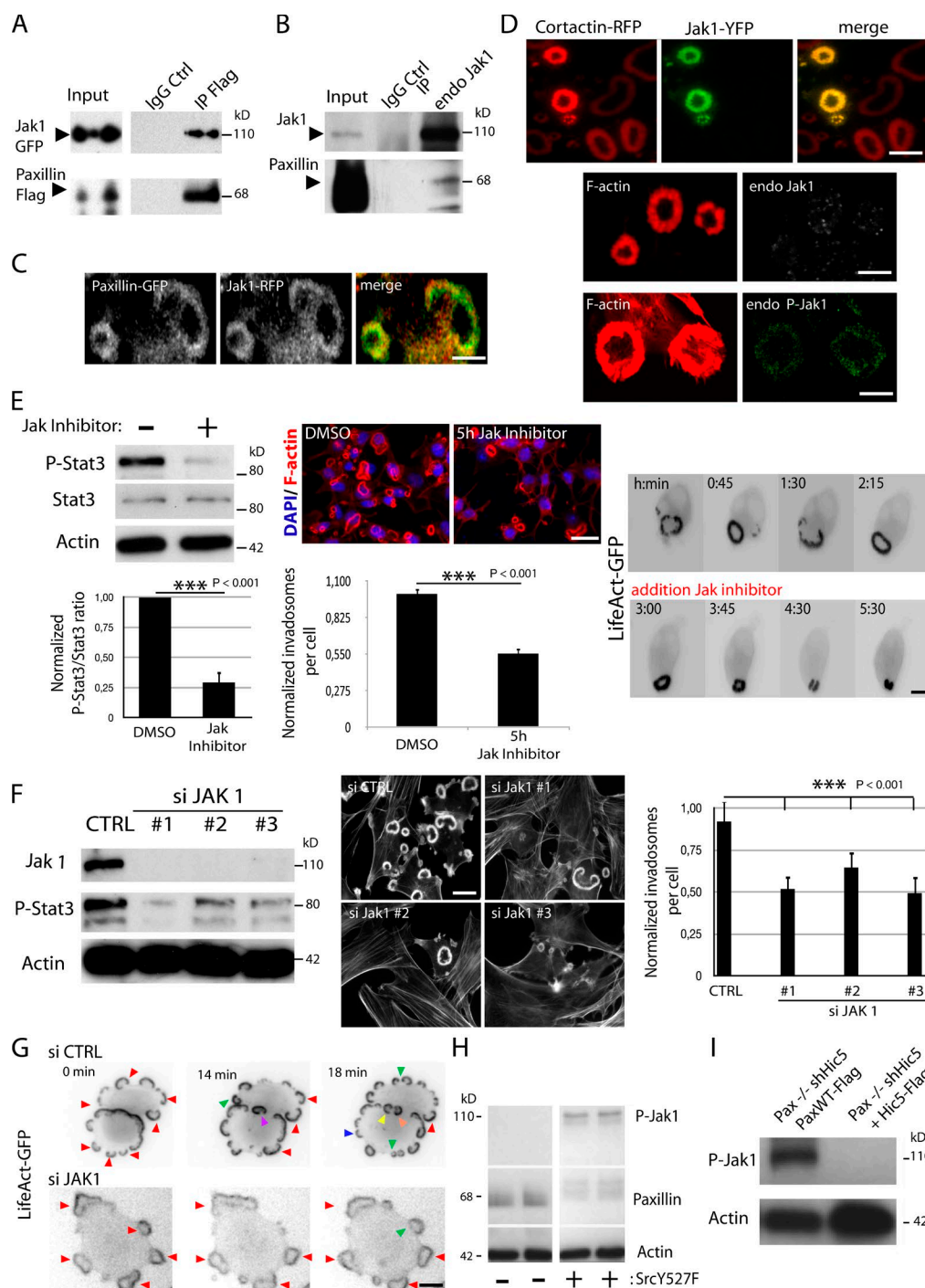
JAK1 staining after JAK1 silencing or Jak1 inhibitor treatment (Figs. 5 D and S4, A and B). A JAK1–paxillin interaction was confirmed by the colocalization of JAK1-RFP and paxillin-GFP, as imaged by confocal microscopy (Fig. 5 C). To understand the function of JAK1 in the invadosome, MEF-SrcY527F cells were treated with Jak inhibitor I (also called P6) for a few hours. This treatment led to a specific decrease of its substrate, signal transducer and activator of transcription 3 (STAT3; Fig. 5 E). It also induced a significant decrease in the number of invadosome rings per cell (Fig. 5 E). The invadosome dynamics were reminiscent of that observed in SrcY527F paxillin-depleted MEF cells (Fig. 3 F), as revealed by the decrease in their turnover and size (Fig. 5 E). As Jak inhibitor I is not specific for JAK1 but targets several members of Jak family, we specifically silenced JAK1. We validated three siRNAs that efficiently silenced JAK1, leading to a decrease in the phosphorylation of its substrate, STAT3 (Fig. 5 F). In MEF-SrcY527F cells, JAK1 depletion induced a significant decrease of invadosome formation, confirming our pharmacologic approach, and an increase of stress fibers (Fig. 5 F). The remaining invadosomes presented a slow turnover in comparison to control cells like those observed in SrcY527F paxillin-depleted MEF or in SrcY527F-pax⁻/⁻ shHic-5 cells expressing paxillin-ΔLIM (Fig. 5 G). Importantly, JAK1 phosphorylation increased after invadosome induction upon SrcY527F expression (Fig. 5 H) and was dependent on the presence of paxillin but not Hic-5, as observed in SrcY527F pax⁻/⁻ shHic-5 cells reexpressing either pax-WT-Flag or Hic-5-WT-Flag (Fig. 5 I). Thus, paxillin controls invadosome dynamics through its ability to interact with the kinase JAK1 and regulates its activation.

Hic-5 controls the recruitment of exocyst regulator IQGAP1 in invadosomes

The interaction of Hic-5 with IQGAP1 supports the preferential role of Hic-5 in the degradative function of invadosomes (Fig. 4 B). Indeed, IQGAP1 is required for the exocyst-dependent delivery at the cell surface of MT1-MMP and for the ECM degradation activity of invadosomes (Sakurai-Yageta et al., 2008). In HEK293 cells expressing both IQGAP-GFP and Hic-5-WT-Flag or pax-WT-Flag, Hic-5-WT-Flag interacted more strongly with IQGAP1-GFP than pax-WT-flag (Fig. 6 A), confirming IQGAP1–Hic-5 interaction. Moreover, endogenous Hic-5 coimmunoprecipitated with endogenous IQGAP1 from MEF cells overexpressing SrcY527F (Fig. 6 B). IQGAP1-GFP colocalized with Hic-5-Flag in invadosomes (Fig. 6 C), validating the Hic-5/IQGAP1 interaction found by mass spectrometry and coimmunoprecipitation. TIRF imaging showed the accumulation of IQGAP1-GFP into invadosome structures labeled by the specific marker RFP-cortactin (Fig. 6 D). Similarly, endogenous IQGAP1 was immunodetected in invadosomes (Fig. 6 D). The loss of signal upon IQGAP1 silencing in MEF-SrcY527F cells confirmed the specificity of the antibody used (Fig. S4 C).

Next, we addressed the question of whether Hic-5 affects IQGAP1 recruitment in invadosomes. Hic-5 depletion significantly decreased IQGAP1 recruitment to invadosomes compared with control conditions (Fig. 6 E), a decrease that was rescued by reexpression of Hic-5-WT-Flag in SrcY527F Hic-5⁻/⁻ cells (Fig. 6 E). Therefore, Hic-5 is required to localize IQGAP1 in invadosomes. As shown previously (Sakurai-Yageta et al., 2008), IQGAP1 silencing led to a decrease of matrix degradation (Fig. S5 A) caused by a decrease in the accumulation of endogenous MT1-MMP at the surface of invadosomes

2011; Albrengues et al., 2014; Orgaz et al., 2014). In HEK293 cells transfected with JAK1-GFP and pax-WT-Flag, JAK1-GFP coimmunoprecipitated with pax-WT-Flag (Fig. 5 A), confirming the interaction seen by mass spectrometry. Moreover, endogenous paxillin was coimmunoprecipitated with endogenous JAK1 from MEF cells overexpressing SrcY527F (Fig. 5 B). We addressed the question of whether the paxillin/JAK1 complex serves to recruit JAK1-GFP into invadosomes. Total internal reflection fluorescence (TIRF) imaging showed the accumulation of JAK1-GFP into invadosome structures labeled by the specific marker RFP-cortactin (Fig. 5 D). Endogenous JAK1 was also localized in invadosome rings as validated by the decrease of

Figure 5. **JAK1 interacts and colocalizes with paxillin in invadosome rings and regulates their assembly.** (A) The specific coimmunoprecipitation of pax-WT-Flag and JAK1-GFP, transfected in HEK 293 cells, showed the interaction of these two proteins. (B) Immunoprecipitation of endogenous JAK1 in MEF-SrcY527F cells is associated with a specific coimmunoprecipitation of paxillin in comparison to rabbit polyclonal IgG control. (C) Confocal imaging of MEF-SrcY527F cells expressing paxillin-GFP and JAK1-RFP showed their colocalization. (D) TIRF imaging of MEF-SrcY527F cells expressing RFP-cortactin and JAK1-YFP showed the localization of this kinase in invadosome (top). Confocal imaging of endogenous JAK1 (total JAK1 or phospho-JAK1) revealed its accumulation in invadosomes (bottom). (E) Treatment with 25 µm Jak inhibitor I (P6) induced a decrease in STAT3 phosphorylation (left) associated with a significant decrease in invadosome formation (middle; $n = 3$; 350 cells counted per condition). Representative images extracted from a time series of MEF-SrcY527F cells expressing LifeAct-GFP and treated with 25 µm Jak inhibitor I (right). (F) Western blot of cell lysates from MEF-SrcY527F cells treated with control or JAK1 siRNA (left). F-actin staining of cells treated by these different siRNAs shows that JAK1 silencing significantly reduces invadosome formation (middle), as quantified at the right ($n = 4$, 500 cells counted per conditions), and induces the formation of stress fibers (middle). ***, $P < 0.001$. (G) Representative images extracted from the time series of MEF-SrcY527F expressing LifeAct-GFP revealed long-lasting large rings (red arrowhead) after JAK1 silencing in comparison to dynamic invadosome (multicolored arrowheads) in control condition. (H) Western blot analysis revealed the increase in JAK1 phosphorylation in response to the expression of constitutively activated mutant of Src, Src Y527F. (I) Western blot analysis of MEF-SrcY527F pax$^{-/-}$ shHic-5 cells expressing Hic-5 or pax-WT-Flag increases JAK1 phosphorylation. All graphs presented as means ± SD. Differences with a probability level $P < 0.05$ were considered significant in one-way ANOVA. Bars: (C) 3 µm; (D) 5 µm; (F and G) 10 µm.
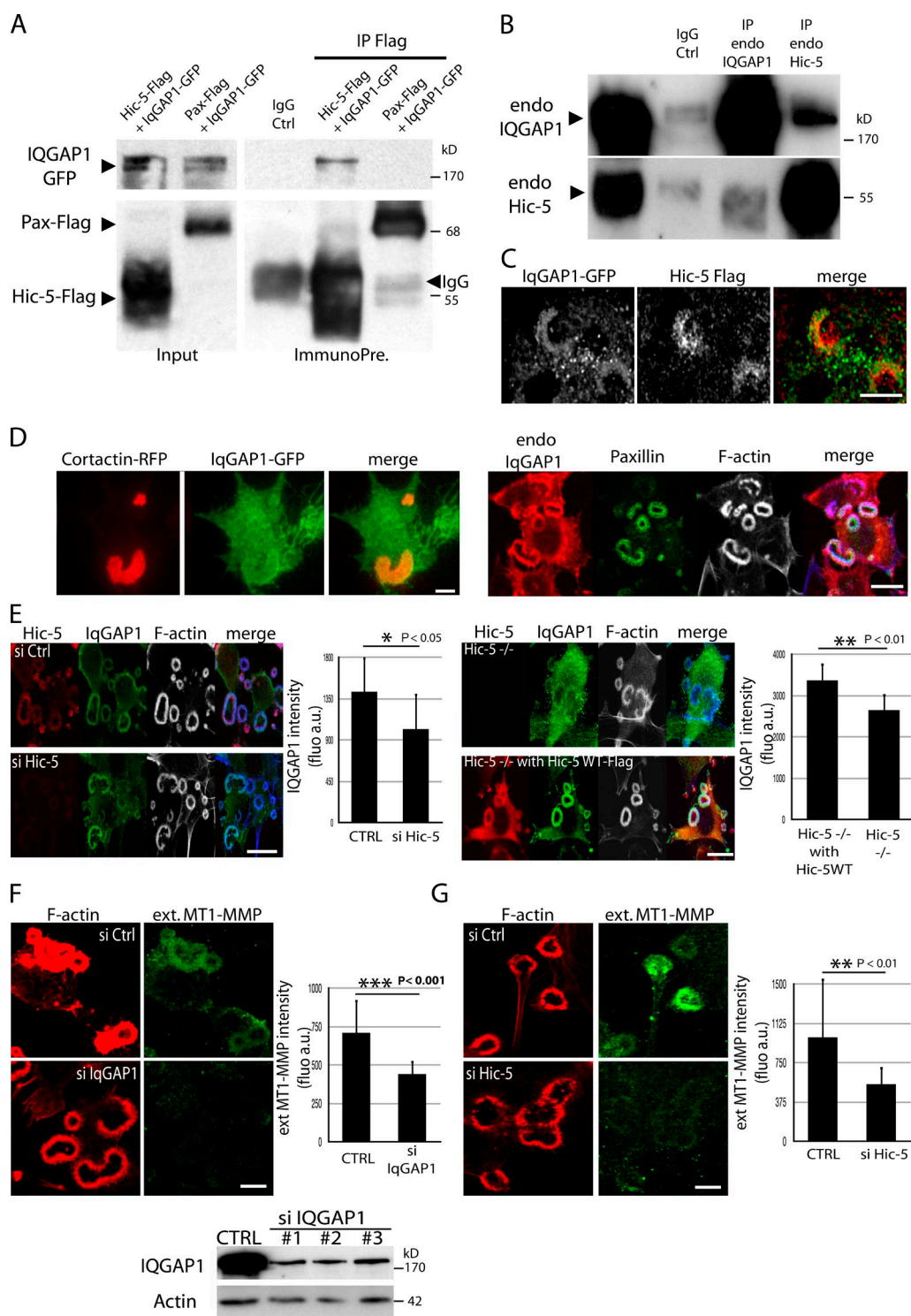
Figure 6. **Hic-5 interacts specifically with IQGAP1 and controls its recruitments to invadosomes.** (A) The specific coimmunoprecipitation of Hic-5-WT-Flag and IQGAP1-GFP, transfected in HEK 293 cells, showed the specific interaction of these two proteins. (B) Immunoprecipitation of endogenous IQGAP1 or Hic-5 in MEF-SrcY527F cells is associated with the respective specific coimmunoprecipitation of Hic-5 and IQGAP1, in comparison to IgG control. (C) Confocal imaging of MEF-SrcY527F cells expressing Hic-5-Flag and IQGAP1-GFP showed their colocalization. (D) TIRF imaging of MEF-SrcY527F cells shows IQGAP1-GFP localization in invadosome revealed by RFP-cortactin (left). Confocal imaging of endogenous IQGAP1 also revealed its accumulation in invadosomes (right). (E) Quantitative confocal imaging showed that Hic-5 silencing is associated with a decrease in endogenous IQGAP1 recruitment in invadosomes (left; $n = 3$; 60 invadosomes per condition). Moreover, MEF-SrcY527F Hic-5$^{-/-}$ cells presented a representative decrease in IQGAP1 recruitment in invadosomes, in comparison with MEF-SrcY527F Hic-5$^{-/-}$ cells reexpressing Hic-5-WT-Flag ($n = 3$; 55 invadosomes per condition). *, $P < 0.05$; **, $P < 0.01$. (F) Western blot of cell lysates from MEF-SrcY527F cells treated with control or IQGAP1 siRNA (top). Quantitative confocal imaging shows that IQGAP1 silencing decreases plasma membrane accumulation of MT1-MMP in invadosomes ($n = 3$; 60 to 70 invadosomes per condition; bottom). ***, $P < 0.001$; **, $P < 0.01$. (G) Quantitative confocal imaging shows that Hic-5 silencing mimics IQGAP1 silencing in MT1-MMP accumulation at the surface of invadosomes ($n = 3$; 50 invadosomes per condition). All graphs presented as means ± SD. Differences with a probability level $P < 0.05$ were considered significant in one-way ANOVA. Bars: (C–E) 8 µm; (F and G) 5 µm.
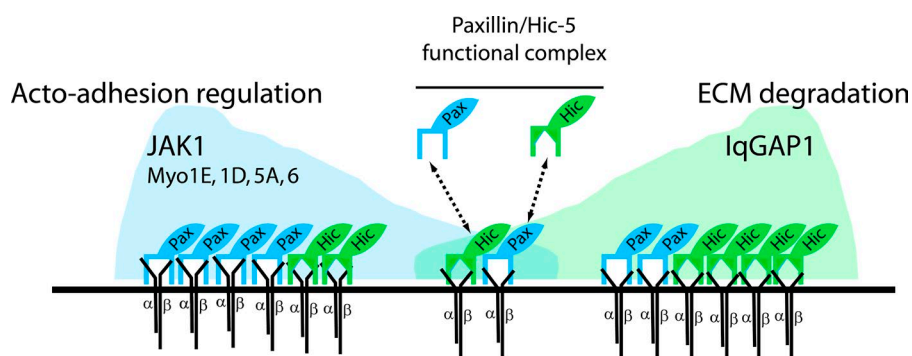
Figure 7. **Scheme of the functional cooperation of paxillin and Hic-5 in the coupling of acto-adhesive and ECM-degradation activities of invadosomes.**

(Figs. 6 F and S5 B). Hic-5 depletion also significantly decreased the accumulation of MT1-MMP in invadosomes (Fig. 6 G). Therefore, in addition to its redundant activity with paxillin in invadosome formation, by recruiting IQGAP1, Hic-5 is a new molecular link that couples adhesion with the exocytic delivery of MT1-MMP. Our results show that Hic-5 participates in the coupling between acto-adhesive and ECM-degradation activities occurring in fully functional invadosomes.

Discussion

An optimal balance of paxillin or Hic-5 signaling controls the invasive migration of breast cancer cells (Deakin and Turner, 2011). To explore the role of each paxillin family member, a combination of loss-of-function and silencing strategies showed the redundancy of paxillin and Hic-5 in the formation of invadosomes. In addition to this redundancy, we demonstrated their specific functions. Paxillin primarily regulates the acto-adhesive properties of invadosomes through the regulation of its new interactor, JAK1. Hic-5 preferentially regulates ECM degradation by interacting with IQGAP1. Finally, redundant and specific paxillin and Hic-5 functions support new insights into the coupling between the acto-adhesive machinery and ECM degradation.

Essential and redundant functions of paxillin and Hic-5 in invadosomes

The yeast model, devoid of integrins, revealed the mechano-regulatory role of the paxillin yeast homologue, Pxl-1p, while coordinating Rho activity and the acto-myosin ring during cytokinesis (Ge and Balasubramanian, 2008; Pinar et al., 2008). In mammals, numerous studies have shown that paxillin-like activity (from paxillin, Hic-5, or leupaxin) regulates the lifespan of adhesive structures (Webb et al., 2004; Zaidel-Bar et al., 2007; Badowski et al., 2008), whereas its implication during the formation process is poorly understood. By coupling genetic and reverse-genetic approaches, our data show that paxillin and Hic-5 are also essential for the assembly, acto-adhesive, and ECM-degradation functions of invadosomes.

Integrating paxillin and Hic-5 redundancy could explain previous discrepancies in paxillin functions in invadosomes. Indeed, paxillin silencing disorganizes the invadosome belt into small clusters in osteoclasts (Badowski et al., 2008). Pax−/− osteoclasts are characterized by highly organized peripheral invadosome belts but are poorly functional in supporting efficient bone-degrading activity (Zou et al., 2012). This discrepancy could be explained by the fact that acute depletion mediated by siRNA could not allow an adaptive response and instead changed the paxillin/Hic-5 ratio (Fig. 3 A). It has been shown that paxillin and Hic-5 have distinct functions in breast cancer cell morphology but without excluding cooperative action (Deakin and Turner, 2011). The paxillin–Hic-5 redundancy suggests that these proteins can work cooperatively and thus form a functional complex. Therefore, the question of the molecular basis of this complex is raised. No direct interaction in vitro between these two proteins has been reported despite their potential ability to homodimerize through their LIM domain (Feuerstein et al., 1994). However, paxillin and Hic-5 can be purified in the same complex in response to mechanical load (Guignandon et al., 2006). Paxillin and Hic-5 redundancy based on the same molecular mobility, partners, and sites of action supports this concept of functional complex (Fig. 1). Then, exchange of paxillin by Hic-5 will induce differential functions in the same site of action (Fig. 7). The integration of both the redundancy and specificities of paxillin and Hic-5 in a functional complex supports a new model of the coupling between acto-adhesive machinery and ECM degradation in invadosomes.

Functions and cooperativity of LIM and LD domains in invadosomes

Based on paxillin–hic-5's redundancy, their high level of homology, and the absence of invadosomes in cells depleted of paxillin and Hic-5, a large structure–function study was possible to determine the different functions of the LD and LIM domains that were poorly known in invadosomes. The function of paxillin LIM domains was first related to localizing paxillin to focal adhesions (Brown et al., 1996) in response to mechanical constraints (Smith et al., 2013; Watanabe-Nakayama et al., 2013). The fact that LIM domains are important for paxillin's recruitment to invadosomes, their morphology, dynamics, and ECM degradation is reminiscent of the effect of the myosin II inhibitor blebbistatin, which affects invadosome morphology and decreases ECM proteolytic activity (Alexander et al., 2008). This finding suggests that the LIM domains could affect the mechanical properties of the acto-adhesive machinery that regulates ECM degradation.

Even in the absence of LIM domains, all LD domains were sufficient to localize paxillin in invadosomes and restore their formation. These LD motifs have been implicated in numerous interactions with adhesion components or regulators such as FAK/Pyk2, Src, p130Cas, talin, and vinculin (Deakin and Turner, 2008). We showed that all LD domains are important in restoring invadosome ring formation, even the less-characterized LD3 and LD5 domains, whereas focal adhesion dynamics has been shown to be mostly dependent on LD2 and LD4, which bind FAK. The subsequent question was to determine whether the LDs presented coordinated binding activity. Surprisingly, repositioning of LD3

and LD5 negatively affected paxillin's ability to restore invadosome formation, indicating the cooperative function of LD motifs and confirming previous models suggesting that the LD motifs create a ternary structure that supports interaction with specific proteins (Bertolucci et al., 2005).

Paxillin preferentially regulates invadosome formation and dynamics

A comparison of reverse-genetic and siRNA approaches revealed that paxillin preferentially acts on the regulation of the acto-adhesive machinery in invadosomes (Fig. 3). Surprisingly, Hic-5 silencing increased the mean number of invadosome rings per cells. As shown by the rescued expression of Hic-5 in SrcY527F pax$^{-/-}$ shHic-5 cells, this was not because of a potential negative role of Hic-5 in invadosome formation but was rather caused by an increase in the paxillin/Hic-5 ratio (Fig. 3 A). The function of paxillin on assembly and disassembly of invadosomes is reminiscent of the pleiotropic activity of its main kinase c-Src in podosomes (Luxenburg et al., 2007; Destaing et al., 2008). The preferential activity of paxillin on invadosome dynamics is supported by the identification of its specific interactors, such as cytoskeleton regulators and myosin motors (myo1D/E, myo5, and myo6). A major surprise of this paxillin interactomics is the interaction with JAK1, a new regulator of cell contractility. Although this kinase modulates acto-myosin contractility during tumor progression (Sanz-Moreno et al., 2011; Albrengues et al., 2014; Orgaz et al., 2014), the precise link between acto-adhesive structures and JAK has not been explained. The identification of a paxillin–JAK1 interaction is the first molecular mechanism supporting Jak functions in invasive adhesive structures.

Hic-5 regulates ECM degradation by controlling IQGAP1 recruitment in invadosomes

We showed that Hic-5 plays a key role in ECM degradation, which is in line with results from previous studies that have demonstrated that Hic-5 promotes increased ECM degradation in TGF-β–induced invadopodia formation (Pignatelli et al., 2012). The identification of the IQGAP1 as a specific interactor of Hic-5 seems to be a critical element in explaining the functional relationship between Hic-5 and ECM degradation. Indeed, Sakurai-Yageta et al. (2008) have shown that the CDC42 effector IQGAP1 is an important player in the coordination between actin polymerization and MT1-MMP secretion in invadosomes. In invadosomes, IQGAP1 can directly bind two subunits of the exocyst complex, sec3 and sec8, and it therefore drives MT1-MMP relocalization in invadopodia (Sakurai-Yageta et al., 2008).

Collectively, our work suggests that the integration of paxillin and Hic-5 redundancy and specificities in a functional complex support new molecular insights that explain the coupling between the acto-adhesive machinery and ECM degradation in invadosomes.

Materials and methods

Antibodies and reagents

Mouse monoclonal antibodies against paxillin (clone 349) and Hic-5 (clone 34) were obtained from BD. Rabbit monoclonal anti-Src (32G6), rabbit polyclonal anti-JAK1, anti–phospho-JAK1 (1022/1023), anti-STAT3, and anti–phospho-STAT3 antibodies were purchased from Cell Signaling Technology. For immunolocalization of endogenous proteins, the goat polyclonal antibody anti-JAK1 was purchased from R&D Systems (AF602). Mouse monoclonal anti-leupaxin (clone Leu133), mouse monoclonal anti-actin and anti-Flag (clone M2), and rabbit polyclonal anti-vinculin antibodies were obtained from Sigma-Aldrich. The rabbit polyclonal antibody against MT1-MMP was purchased from Abcam (Ab51074). The different IgG controls were obtained from Abcam. A rabbit polyclonal antibody against IQGAP1 was purchased from Santa Cruz Biotechnology, Inc. HRP-conjugated goat anti–mouse and goat anti–rabbit antibodies were purchased from Bio-Rad Laboratories and Jackson ImmunoResearch Laboratories, Inc., respectively. Alexa Fluor 488–, 546–, and 647–labeled phalloidin and Alexa Fluor 488–, 546–, and 647–conjugated secondary antibodies (goat anti–mouse and goat anti–rabbit) were purchased from Invitrogen. JAK inhibitor I (Insolution JAK Inhibitor I or P6), which inhibits multiple members of the JAK family, was used at 25 µM and was purchased from EMD Millipore.

siRNAs (ON-TARGETplus) targeting paxillin (L-042346-00), Hic-5 (L-041105-01), and IQGAP1 (L-040589-01) were purchased from Thermo Fisher Scientific and transfected with Lipofectamine RNAiMAX (Invitrogen) following the standard protocol. Knockdown was performed via two rounds of siRNA transfection at 24-h intervals. The following siRNA (Dharmacon) sequences were used: control (5′-UGGUUUACAUGUCGACUAA-3′); on target-SMART pool Paxillin (ref. 19303: 5′-GGCAAAGCGUACUGUCGUA-3′; 5′-GUGUAC AGCUCCAGUGCUA-3′; 5′-UGGCGUCACUGUCAGAUUU-3′; 5′-GAACUUGACCGGCUGUUAC-3′); on target-SMART pool Hic-5 (ref. 21804: 5′-UCUGUGAGCUAGACCGUUU-3′; 5′-GGGAAU GCCUUGCGCCCCUU-3′; 5′-AGUGCUACUUUGAGCGCUU-3′; 5′-GGGACAAGGAUCAUCUAUA-3′); on target JAK1 set (ref. 16451: #1, 5′-GAAAAUGAAUUGAGUCGAU-3′; #2, 5′-GAAAUC ACCCACAUUGUAA-3′; #3, 5′-CGCAUGAGGUUCUACUUUA-3′); and on target IQGAP1 set (ref. 29875: #1, 5′-AGACAGGAGAGG CGAGCAA-3′; #2, 5′-CUAUGAUUGUGGUCCGAAA-3′; #3, 5′-CAAGAUGACAAACGCUAAA-3′).

Plasmids

pBabe-Flag paxillin (WT and mutated forms ΔLD1, ΔLD2, ΔLD3, ΔLD4, ΔLD5, and ΔLIM) vectors were provided by S. Vande Pol (University of Virginia, Charlottesville, Virgina; Wade et al., 2011). For the pBABE-Flag LD3_ΔLD3 and pBABE-Flag LD5_ΔLD5 constructs, linkers (Eurofins) with the coding sequences of LD3 (forward: 5′-AATTCAGTGTGGAGAGCCTGCTGGATGAGCTGGAGAGCT CTGTGG-3′; reverse: 5′-AATTCCACAGAGCTCTCCAGCTCATCC AGCAGGCTCTCCACACT-3′) and LD5 (forward: 5′-AATTCCAGC TGGACACCATGCTGGGAAGTCTGCAGTCTGACCTGG-3′; reverse: 5′-AATTCCAGGTCAGACTGCAGACTTCCCAGCATGGTG TCCAGCTGG-3′) were inserted into an EcoRI site located at the N-terminal end of the pBABE-Flag ΔLD3 and pBABE-Flag ΔLD5 vectors, respectively, using EcoRI restriction enzyme and T4 DNA ligase. For the pBabe Hic-5 construct, a linker (Eurofins) with the coding sequence of the FLAG epitope (forward: 5′-GATCCATGGACTACA AAGACGATGACGACAAGG-3′; reverse: 5′-AATTCCTTGTCGTCA TCGTCTTTGTAGTCCATG-3′) was inserted into the N-terminal end of Hic-5 using EcoR1 and BamH1 restriction enzymes and T4 DNA ligase. For the pBabe Hic-5-GFP construct, the GFP coding sequence was PCR-amplified (forward: 5′-CAAGGATCCATGGTGAGCAAG GGCGAGG-3′; reverse: 5′-CGTGAATTCCTTGTACAGCTCGTC CATGC-3′) from the original pEGFP-C1 vector (BD) and inserted into the N-terminal of Hic-5 using EcoR1 and BamH1 restriction enzymes and T4 DNA ligase. *Mus musculus* SrcY527F mutant was cloned into

pMX retroviral vector (Destaing et al., 2010). JAK1-YFP and IQG AP1-GFP were gifts from C. Lamaze (Institute Curie, Paris, France) and P. Chavrier (Institute Curie, Paris, France), respectively. The pBabe paxillin-GFP vector was previously described (Badowski et al., 2008).

Cell culture, infection, and silencing experiments

Fibroblasts were isolated from mice from the age of embryonic day 12 to postnatal day 1 as described recently (Destaing et al., 2010). Cells were grown in DMEM (containing glutamine) + 10% FBS + 1% penicillin/streptomycin supplement. cDNAs were delivered via a retroviral transduction after packaging in Phoenix-Eco cells or Phoenix-Ampho cells (ATCC). Supernatant containing viral particles from such cells was harvested and filtered, and after addition of 8 µg/ml polybrene (Sigma-Aldrich), was used to transduce fibroblasts. MEF cells expressing a constitutively active mutant of Src, SrcY527F, were produced as described previously (Destaing et al., 2010).

Pax$^{-/-}$ shCT and pax$^{-/-}$ shHic-5 cells were provided by S. Vande Pol (University of Virginia, Charlottesville, VA). To summarize, fibroblasts that are derived from paxillin-null ES cells (Wade et al., 2002) were stably transduced with shRNA against HIC5 delivered retrovirally, to obtain a stable knockdown of HIC5 by >95% (Wade et al., 2011). As previously described, Hic-5$^{-/-}$ cells were obtained from Hic-5$^{-/-}$ embryos (Kim-Kaneyama et al., 2012) and were provided by J.R. Kim-Kaneyama (Showa University School of Medicine, Shinagawa-ku, Tokyo, Japan). The cell lines and the HEK293 cells were maintained in DMEM supplemented with 10% FCS and 1% penicillin/streptomycin.

Reexpression experiments with pax-WT, Hic-5-WT, and the other paxillin's mutated forms in pax$^{-/-}$ shHic-5 cells were performed via retroviral infection using pBabe vectors. In most experiments, cDNAs were delivered via retroviral transduction after packaging in Phoenix-Eco or Phoenix-Ampho cells. For transient transfections, constructs were delivered with Lipofectamine 2000 (Invitrogen) according to the manufacturer's instructions. MEF-SrcY527F (10^5) cells were plated 24 h before transfection in two-well cell culture Lab-Tek chambers.

Immunofluorescence microscopy, live-imaging, and FRAP

Cells were fixed for 10 min with 4% PFA in PBS, permeabilized for 10 min (0.2% Triton X-100), and blocked for 10 min in 4% BSA in PBS. Cells were then incubated for 1 h at RT with primary antibodies. For specific staining of MT1-MMP at the plasma membrane, cells were incubated with primary antibody without any previous permeabilization. Secondary antibodies were then added for 1 h at RT. Coverslips were permanently mounted in Mowiol (EMD Millipore) containing 4′,6-diamidino-2-phenylindole.

Imaging of fixed cells was performed on a confocal microscope (LSM510 3.2 software; ZEISS) equipped with a Plan Neo-Fluor 40× (NA 1.2, oil) or Plan-Apochromat 100× (NA 1.4, oil, DIC) objective. The images were then processed with ImageJ software. For quantitative confocal imaging, all images were acquired with the same optical path and setup detection and quantified without any ImageJ processing.

For live imaging, LifeAct-TagRFP–expressing cells were seeded overnight at subconfluent densities in serum-coated Lab-Tek coverglass. During imaging, cells were placed on a heated 37°C stage (ZEISS), with a CO$_2$-independent medium (Life Technologies) and imaged with an Axiovert 200M microscope (ZEISS) equipped with a Coolsnap HQ2 camera (Photometrics) and a Plan Neo-Fluor 40× (NA 1.2) objective. Images were sampled with MetaMorph software (Molecular Devices). Time-lapse videos were then processed with ImageJ software.

TIRF microscopy was performed with an Axiovert 200M microscope equipped with a Coolsnap HQ2 camera (Photometrics), 100× (NA 1.4, oil) Plan Apochromat objectives, and a TIRF 1 slider (ZEISS). Images were acquired with MetaMorph software and processed with ImageJ software.

For fluorescence recovery after photobleaching experiments (FRAP), a confocal microscope (LSM 510; ZEISS) equipped with a Plan Neo-Fluor 40× (NA 1.2, oil) objective was used. To analyze and compare recovery kinetics, FRAP measurements were fitted to a single exponential curve, $I_{(t)} = I_{(0)} + k_1 e^{-k2t}$ (performed with ZEN software; ZEISS) to determine the characteristic time of recovery.

ECM degradation assays

Coverslips were coated with 1 mg/ml gelatin-Oregon green, fixed with 4% paraformaldehyde/0.5% glutaraldehyde for 30 min at 4°C, washed with 30 mg/ml sodium borohydride in PBS, sterilized with 70% ethanol, and washed with PBS. The cells were seeded on these coverslips for 15 h, fixed, and observed with an Axiovert 200 M microscope equipped with a MicroMax 5-MHz and LD plan 10× (NA 0.25) objective. The quantification of cells' degradation ability was established by calculating the total degradation area per field of view after setting a low-intensity threshold on gelatin-captured images with ImageJ software.

Western blotting

Whole cell lysates were prepared in buffer containing 50 mM Tris-HCl, pH 7.4, 150 mM NaCl, 0.5% Triton X-100, 0.5% (wt/vol) sodium deoxycholate, 1 mM NaF, 2 mM MgCl$_2$, 1 mM orthovanadate (Na$_3$VO$_4$), and 4% (vol/vol) protease inhibitor cocktail (complete EDTA-free; Roche Diagnostics). 30 µg of proteins from each cell lysate was subjected to SDS-PAGE, transferred to nitrocellulose membranes, and probed with primary antibodies. Immunologic detection was achieved with HRP-conjugated goat anti–mouse or goat anti–rabbit secondary antibody. Peroxidase activity was visualized by ECL (West Pico Signal; Thermo Fisher Scientific) using a ChemiDoc MP imaging system (Bio-Rad Laboratories). Densitometric quantification of the bands was performed using Image Lab (Bio-Rad Laboratories). As a control, detection of actin was also performed. Stripping was performed in 60 mM Tris, pH 6.8, 2% SDS, and 100 mM β-mercaptoethanol solution and incubated at 50°C for 30 min, washed three times, and resaturated before probing with anti-Src and anti-STAT3. For quantification of different experiments, each quantified protein was normalized to actin, and then all values were normalized to the control values.

Quantitative real-time PCR

Total RNA was isolated using the NucleoSpin RNA II kit (MACHEREY-NAGELl) according to the manufacturer's instructions. 1 µg RNA was reverse-transcribed using the SuperScript VILO kit (Thermo Fisher Scientific). PCR amplification of the cDNA from the reverse transcription reaction was performed using specific primer pairs for mouse *paxillin* (forward: 5′-GAGCAGTCCGCAGCGAGTCA-3′; reverse: 5′-ACG GCCGCTCTCCATCCACTC-3′), mouse *Hic-5* (forward: 5′-CGATGT GGCTTCTGTAACCAAC-3′; reverse: 5′-ACCCTCTTCTCCAAA AGGCTC-3′), and mouse *leupaxin* (forward: 5′-TGCCTCCCAAAA CCTCAGCAGC-3′; reverse: 5′-TCCTGCTGGTCTGGCAAGGGT-3′). Quantitative real-time PCR was performed with GoTaq^R QPCR Master Mix (Promega) in a 25-µl reaction on a thermal cycler (C-1000 Touch; Bio-Rad Laboratories). Ct values were determined with the same software, and normalization was conducted with housekeeping genes *actin*, *RanBP1*, *GAPDH*, and *ATP50*, which yielded similar results. The expression levels of each target gene in the siRNA-treated cells were calculated with GAPDH as a reference gene and compared with the controls.

Immunoprecipitation

Cells that stably expressed Flag fusion proteins were lysed with a buffer containing 50 mM Hepes, pH 7.5, 120 mM NaCl, 5% (vol/vol) glycerol, 1 mM Na$_3$VO$_4$, 1 mM DTT, and 4% (vol/vol) protease inhibitor cocktail (complete EDTA-free; Roche) and were incubated under rotation

for 30 min at 4°C. The cell debris was removed by centrifugation at 1,000 rpm for 10 min at 4°C. Cell lysates were precleared using IgG Sepharose beads (GE Healthcare) for 30 min under rotation at 4°C. The supernatant was collected and incubated with anti-Flag M2 affinity gel under rotation for 2.5 h at 4°C. Beads that contained Flag proteins were washed three times with the lysis buffer. After centrifugation, the pellets were subjected to SDS-PAGE and silver staining for protein detection. The same samples were also used for proteomic analyses.

To validate paxillin's interaction with JAK1 and Hic-5 binding to IQGAP1, HEK293 cells were cotransfected (Lipofectamine 2000; Invitrogen) with constructs encoding pax-WT-Flag/JAK1-WT-YFP and IAGAP1-WT-GFP/Hic-5-WT-Flag or pax-WT-Flag. Their interactions were analyzed by immunoprecipitation as previously described, using anti-Flag M2 bound to G-protein Dynabeads (Invitrogen). Interactions were confirmed with endogenous proteins. MEF-SrcY527F cells were lysed with a buffer containing 20 mM Hepes, pH 7.5, 0.5% IGEPAL, 100 mM NaCl, 1 mM Na_3VO_4, and 4% (vol/vol) protease inhibitor cocktail (complete EDTA-free; Roche). 500 µg of lysates was incubated under rotation for 20 min at 4°C, passed a few times through a syringe, and centrifuged at 10,000 rpm for 15 min at 4°C. Cell lysates were precleared using IgG Sepharose beads (GE Healthcare) for 30 min under rotation at 4°C. The supernatant was collected and incubated with rabbit polyclonal anti-JAK1 (Cell Signaling), rabbit polyclonal anti-IQGAP1 (Santa Cruz Biotechnology, Inc.), mouse monoclonal anti–Hic-5, or the same amount of the rabbit IgG control (Abcam) or mouse IgG1 isotype control (Abcam) under rotation overnight at 4°C before adding protein G Sepharose beads. After 1-h incubation under rotation at 4°C, beads were washed four times for 5 min each.

Proteomic analyses

After solubilizing in Laemmli buffer, eluted proteins were separated by SDS-PAGE (NuPAGE; Invitrogen) and stained with Coomassie blue R-250 (Bio-Rad Laboratories). Bands corresponding to heavy and light chains of immunoglobulin were separated, and the remaining parts of the lane were pooled. Proteomic analyses were then performed with liquid chromatography/tandem mass spectrometry (LC-MS/MS) as previously described. After in-gel digestion of protein using trypsin, the resulting peptides were analyzed by nano-LC-MS/MS (Ultimate U3000, Dionex, and LTQ-Orbitrap Velos pro; Thermo Fisher Scientific). Peptides were sampled on a 300 µm × 5 mm PepMap C18 precolumn and separated on a 75 µm × 250 mm C18 column (PepMap; Dionex). The nano-LC method consisted of a 120-min gradient at a flow rate of 300 nl/min. Mass spectrometry and tandem mass spectrometry data were acquired using Xcalibur (Thermo Fisher Scientific): survey full-scan MS spectra (m/z = 400–1,600) were acquired in the Orbitrap with a resolution of 60.000 after accumulation of 10^6 ions (maximum filling time, 500 ms), and the 20 most intense ions from the MS scan were fragmented by collision-induced dissociation (collision energy 35%) in the LTQ after accumulation of 10^4 ions (maximum filling time, 100 ms). Peptides and proteins were identified through concomitant searches against the Uniprot databank (*Mus musculus* taxonomy) using Mascot software (version 2.5). IRMa software (Dupierris et al., 2009; version 1.31.1) was used to filter the results: conservation of rank 1 peptides, peptide identification false discovery rate <1% (as calculated on peptide scores by using the reverse database strategy), and minimum of one specific peptide per identified protein group. Filtered results were then uploaded into a relational mass spectrometry identification database before performing a compilation, grouping, and comparison of the protein groups from the different samples using a homemade tool (hEIDI, version 1.14.3). To discriminate between potential binding partners and unspecific background, results obtained from cell lysates containing the pax-WT, Hic-5-WT, or mutant forms were compared with those obtained with a negative control that contained only IgG (negative control). Proteins were considered to be significantly enriched with the bait protein if (a) they exhibited a spectral count ≥2 in the positive immunoprecipitation and (b) they were not identified in the negative control or at least enriched five times in the positive immunoprecipitation when proteins were identified in the negative control. The spectral count values were calculated as the mean values of three different experiments analyzed by mass spectrometry.

Statistical analysis

Quantitative data (characteristic time of recovery, ECM proteolytic activity, and Western blot quantifications) are presented as means ± SD and statistically analyzed with NCSS 2004 software by one-way analysis of variance (ANOVA). Differences with a probability level P < 0.05 were considered significant. All graphs include standard deviation error bars.

Online supplemental material

Fig. S1 shows morphometric, dynamic, and molecular mobility analyses of invadosomes induced by either pax-Flag-WT or mutant pax-ΔLIM-Flag in SrcY527F pax$^{-/-}$ shHic-5 MEF cells to analyze the function of the paxillin LIM domain in invadosome morphometry and dynamics. Fig. S2 examines the impact of expression of various paxilin mutant proteins on ECM degradation patterns. Fig. S3 analyses the partners of paxillin and in particular the proteins binding to its LD3 and LD5 domains. Fig. S4 shows the localization of endogenous JAK1 and IQGAP1 at invadosomes with or without specific knockdown via siRNA. Fig. S5 presents data on the effects of IQGAP1 silencing on ECM degradation and MT1-MMP presence at the plasma membrane in SrcY527F MEFs. Tables S1, S2, and S3 show the numbers of specific peptides identified for each partner of Hic-5, paxillin, and paxillin mutants, respectively. Online supplemental material is available at http://www.jcb.org/cgi/content/full/jcb.201510036/DC1.

References

Albiges-Rizo, C., O. Destaing, B. Fourcade, E. Planus, and M.R. Block. 2009. Actin machinery and mechanosensitivity in invadopodia, podosomes and focal adhesions. *J. Cell Sci.* 122:3037–3049. http://dx.doi.org/10.1242/jcs.052704

Albrengues, J., G. Meneguzzi, and C. Gaggioli. 2014. Carcinoma-associated fibroblasts in cancer: The great escape [in French]. *Med. Sci. (Paris).* 30:391–397. http://dx.doi.org/10.1051/medsci/20143004012

Alexander, N.R., K.M. Branch, A. Parekh, E.S. Clark, I.C. Iwueke, S.A. Guelcher, and A.M. Weaver. 2008. Extracellular matrix rigidity promotes invadopodia activity. *Curr. Biol.* 18:1295–1299. http://dx.doi.org/10.1016/j.cub.2008.07.090

Badowski, C., G. Pawlak, A. Grichine, A. Chabadel, C. Oddou, P. Jurdic, M. Pfaff, C. Albigès-Rizo, and M.R. Block. 2008. Paxillin phosphorylation controls invadopodia/podosomes spatiotemporal organization. *Mol. Biol. Cell.* 19:633–645. http://dx.doi.org/10.1091/mbc.E06-01-0088

Bertolucci, C.M., C.D. Guibao, and J. Zheng. 2005. Structural features of the focal adhesion kinase-paxillin complex give insight into the dynamics of focal adhesion assembly. *Protein Sci.* 14:644–652. http://dx.doi.org/10.1110/ps.041107205

Boateng, L.R., and A. Huttenlocher. 2012. Spatiotemporal regulation of Src and its substrates at invadosomes. *Eur. J. Cell Biol.* 91:878–888. http://dx.doi.org/10.1016/j.ejcb.2012.06.003

Branch, K.M., D. Hoshino, and A.M. Weaver. 2012. Adhesion rings surround invadopodia and promote maturation. *Biol. Open.* 1:711–722. http://dx.doi.org/10.1242/bio.20121867

Brown, M.C., and C.E. Turner. 2004. Paxillin: Adapting to change. *Physiol. Rev.* 84:1315–1339. http://dx.doi.org/10.1152/physrev.00002.2004

Brown, M.C., J.A. Perrotta, and C.E. Turner. 1996. Identification of LIM3 as the principal determinant of paxillin focal adhesion localization and characterization of a novel motif on paxillin directing vinculin and focal adhesion kinase binding. *J. Cell Biol.* 135:1109–1123. http://dx.doi.org/10.1083/jcb.135.4.1109

Chen, W.T. 1989. Proteolytic activity of specialized surface protrusions formed at rosette contact sites of transformed cells. *J. Exp. Zool.* 251:167–185. http://dx.doi.org/10.1002/jez.1402510206

Deakin, N.O., and C.E. Turner. 2008. Paxillin comes of age. *J. Cell Sci.* 121:2435–2444. http://dx.doi.org/10.1242/jcs.018044

Deakin, N.O., and C.E. Turner. 2011. Distinct roles for paxillin and Hic-5 in regulating breast cancer cell morphology, invasion, and metastasis. *Mol. Biol. Cell.* 22:327–341. http://dx.doi.org/10.1091/mbc.E10-09-0790

Destaing, O., F. Saltel, J.C. Géminard, P. Jurdic, and F. Bard. 2003. Podosomes display actin turnover and dynamic self-organization in osteoclasts expressing actin-green fluorescent protein. *Mol. Biol. Cell.* 14:407–416. http://dx.doi.org/10.1091/mbc.E02-07-0389

Destaing, O., A. Sanjay, C. Itzstein, W.C. Horne, D. Toomre, P. De Camilli, and R. Baron. 2008. The tyrosine kinase activity of c-Src regulates actin dynamics and organization of podosomes in osteoclasts. *Mol. Biol. Cell.* 19:394–404. http://dx.doi.org/10.1091/mbc.E07-03-0227

Destaing, O., E. Planus, D. Bouvard, C. Oddou, C. Badowski, V. Bossy, A. Raducanu, B. Fourcade, C. Albiges-Rizo, and M.R. Block. 2010. β1A integrin is a master regulator of invadosome organization and function. *Mol. Biol. Cell.* 21:4108–4119. http://dx.doi.org/10.1091/mbc.E10-07-0580

Destaing, O., M.R. Block, E. Planus, and C. Albiges-Rizo. 2011. Invadosome regulation by adhesion signaling. *Curr. Opin. Cell Biol.* 23:597–606. http://dx.doi.org/10.1016/j.ceb.2011.04.002

Dupierris, V., C. Masselon, M. Court, S. Kieffer-Jaquinod, and C. Bruley. 2009. A toolbox for validation of mass spectrometry peptides identification and generation of database: IRMa. *Bioinformatics.* 25:1980–1981. http://dx.doi.org/10.1093/bioinformatics/btp301

Feuerstein, R., X. Wang, D. Song, N.E. Cooke, and S.A. Liebhaber. 1994. The LIM/double zinc-finger motif functions as a protein dimerization domain. *Proc. Natl. Acad. Sci. USA.* 91:10655–10659. http://dx.doi.org/10.1073/pnas.91.22.10655

Ge, W., and M.K. Balasubramanian. 2008. Pxl1p, a paxillin-related protein, stabilizes the actomyosin ring during cytokinesis in fission yeast. *Mol. Biol. Cell.* 19:1680–1692. http://dx.doi.org/10.1091/mbc.E07-07-0715

Guignandon, A., N. Boutahar, A. Rattner, L. Vico, and M.H. Lafage-Proust. 2006. Cyclic strain promotes shuttling of PYK2/Hic-5 complex from focal contacts in osteoblast-like cells. *Biochem. Biophys. Res. Commun.* 343:407–414. http://dx.doi.org/10.1016/j.bbrc.2006.02.162

Kim-Kaneyama, J.R., A. Miyauchi, X.F. Lei, S. Arita, T. Mino, N. Takeda, K. Kou, K. Eto, T. Yoshida, T. Miyazaki, et al. 2012. Identification of Hic-5 as a novel regulatory factor for integrin αIIbβ3 activation and platelet aggregation in mice. *J. Thromb. Haemost.* 10:1867–1874. http://dx.doi.org/10.1111/j.1538-7836.2012.04856.x

Linder, S. 2007. The matrix corroded: Podosomes and invadopodia in extracellular matrix degradation. *Trends Cell Biol.* 17:107–117. http://dx.doi.org/10.1016/j.tcb.2007.01.002

Linder, S. 2009. Invadosomes at a glance. *J. Cell Sci.* 122:3009–3013. http://dx.doi.org/10.1242/jcs.032631

Luxenburg, C., D. Geblinger, E. Klein, K. Anderson, D. Hanein, B. Geiger, and L. Addadi. 2007. The architecture of the adhesive apparatus of cultured osteoclasts: From podosome formation to sealing zone assembly. *PLoS One.* 2:e179. http://dx.doi.org/10.1371/journal.pone.0000179

Luxenburg, C., S. Winograd-Katz, L. Addadi, and B. Geiger. 2012. Involvement of actin polymerization in podosome dynamics. *J. Cell Sci.* 125:1666–1672. http://dx.doi.org/10.1242/jcs.075903

Murphy, D.A., and S.A. Courtneidge. 2011. The 'ins' and 'outs' of podosomes and invadopodia: Characteristics, formation and function. *Nat. Rev. Mol. Cell Biol.* 12:413–426. http://dx.doi.org/10.1038/nrm3141

Orgaz, J.L., P. Pandya, R. Dalmeida, P. Karagiannis, B. Sanchez-Laorden, A. Viros, J. Albrengues, F.O. Nestle, A.J. Ridley, C. Gaggioli, et al. 2014. Diverse matrix metalloproteinase functions regulate cancer amoeboid migration. *Nat. Commun.* 5:4255. http://dx.doi.org/10.1038/ncomms5255

Pérez-Alvarado, G.C., C. Miles, J.W. Michelsen, H.A. Louis, D.R. Winge, M.C. Beckerle, and M.F. Summers. 1994. Structure of the carboxy-terminal LIM domain from the cysteine rich protein CRP. *Nat. Struct. Biol.* 1:388–398. http://dx.doi.org/10.1038/nsb0694-388

Pignatelli, J., D.A. Tumbarello, R.P. Schmidt, and C.E. Turner. 2012. Hic-5 promotes invadopodia formation and invasion during TGF-β-induced epithelial-mesenchymal transition. *J. Cell Biol.* 197:421–437. http://dx.doi.org/10.1083/jcb.201108143

Pinar, M., P.M. Coll, S.A. Rincón, and P. Pérez. 2008. *Schizosaccharomyces pombe* Pxl1 is a paxillin homologue that modulates Rho1 activity and participates in cytokinesis. *Mol. Biol. Cell.* 19:1727–1738. http://dx.doi.org/10.1091/mbc.E07-07-0718

Poincloux, R., F. Lizárraga, and P. Chavrier. 2009. Matrix invasion by tumour cells: A focus on MT1-MMP trafficking to invadopodia. *J. Cell Sci.* 122:3015–3024. http://dx.doi.org/10.1242/jcs.034561

Sakurai-Yageta, M., C. Recchi, G. Le Dez, J.B. Sibarita, L. Daviet, J. Camonis, C. D'Souza-Schorey, and P. Chavrier. 2008. The interaction of IQGAP1 with the exocyst complex is required for tumor cell invasion downstream of Cdc42 and RhoA. *J. Cell Biol.* 181:985–998. http://dx.doi.org/10.1083/jcb.200709076

Saltel, F., T. Daubon, A. Juin, I.E. Ganuza, V. Veillat, and E. Génot. 2011. Invadosomes: Intriguing structures with promise. *Eur. J. Cell Biol.* 90:100–107. http://dx.doi.org/10.1016/j.ejcb.2010.05.011

Sanz-Moreno, V., C. Gaggioli, M. Yeo, J. Albrengues, F. Wallberg, A. Viros, S. Hooper, R. Mitter, C.C. Féral, M. Cook, et al. 2011. ROCK and JAK1 signaling cooperate to control actomyosin contractility in tumor cells and stroma. *Cancer Cell.* 20:229–245. http://dx.doi.org/10.1016/j.ccr.2011.06.018

Sattler, M., E. Pisick, P.T. Morrison, and R. Salgia. 2000. Role of the cytoskeletal protein paxillin in oncogenesis. *Crit. Rev. Oncog.* 11:63–76. http://dx.doi.org/10.1615/CritRevOncog.v11.i1.30

Schmeichel, K.L., and M.C. Beckerle. 1994. The LIM domain is a modular protein-binding interface. *Cell.* 79:211–219. http://dx.doi.org/10.1016/0092-8674(94)90191-0

Schmidt, S., I. Nakchbandi, R. Ruppert, N. Kawelke, M.W. Hess, K. Pfaller, P. Jurdic, R. Fässler, and M. Moser. 2011. Kindlin-3-mediated signaling from multiple integrin classes is required for osteoclast-mediated bone resorption. *J. Cell Biol.* 192:883–897. http://dx.doi.org/10.1083/jcb.201007141

Sharma, V.P., R. Eddy, D. Entenberg, M. Kai, F.B. Gertler, and J. Condeelis. 2013. Tks5 and SHIP2 regulate invadopodium maturation, but not initiation, in breast carcinoma cells. *Curr. Biol.* 23:2079–2089. http://dx.doi.org/10.1016/j.cub.2013.08.044

Smith, M.A., E. Blankman, N.O. Deakin, L.M. Hoffman, C.C. Jensen, C.E. Turner, and M.C. Beckerle. 2013. LIM domains target actin regulators paxillin and zyxin to sites of stress fiber strain. *PLoS One.* 8:e69378. http://dx.doi.org/10.1371/journal.pone.0069378

Tarone, G., D. Cirillo, F.G. Giancotti, P.M. Comoglio, and P.C. Marchisio. 1985. Rous sarcoma virus-transformed fibroblasts adhere primarily at discrete protrusions of the ventral membrane called podosomes. *Exp. Cell Res.* 159:141–157. http://dx.doi.org/10.1016/S0014-4827(85)80044-6

Tumbarello, D.A., M.C. Brown, and C.E. Turner. 2002. The paxillin LD motifs. *FEBS Lett.* 513:114–118. http://dx.doi.org/10.1016/S0014-5793(01)03244-6

Turner, C.E., and J.T. Miller. 1994. Primary sequence of paxillin contains putative SH2 and SH3 domain binding motifs and multiple LIM domains: identification of a vinculin and pp125Fak-binding region. *J. Cell Sci.* 107:1583–1591.

Wade, R., J. Bohl, and S. Vande Pol. 2002. Paxillin null embryonic stem cells are impaired in cell spreading and tyrosine phosphorylation of focal adhesion kinase. *Oncogene.* 21:96–107. http://dx.doi.org/10.1038/sj.onc.1205013

Wade, R., N. Brimer, C. Lyons, and S. Vande Pol. 2011. Paxillin enables attachment-independent tyrosine phosphorylation of focal adhesion kinase and transformation by RAS. *J. Biol. Chem.* 286:37932–37944. http://dx.doi.org/10.1074/jbc.M111.294504

Watanabe-Nakayama, T., M. Saito, S. Machida, K. Kishimoto, R. Afrin, and A. Ikai. 2013. Requirement of LIM domains for the transient accumulation of paxillin at damaged stress fibres. *Biol. Open.* 2:667–674. http://dx.doi.org/10.1242/bio.20134531

Webb, D.J., K. Donais, L.A. Whitmore, S.M. Thomas, C.E. Turner, J.T. Parsons, and A.F. Horwitz. 2004. FAK-Src signalling through paxillin, ERK and MLCK regulates adhesion disassembly. *Nat. Cell Biol.* 6:154–161. http://dx.doi.org/10.1038/ncb1094

Zaidel-Bar, R., R. Milo, Z. Kam, and B. Geiger. 2007. A paxillin tyrosine phosphorylation switch regulates the assembly and form of cell-matrix adhesions. *J. Cell Sci.* 120:137–148. http://dx.doi.org/10.1242/jcs.03314

Zou, W., C.J. Deselm, T.J. Broekelmann, R.P. Mecham, S. Vande Pol, K. Choi, and S.L. Teitelbaum. 2012. Paxillin contracts the osteoclast cytoskeleton. *J. Bone Miner. Res.* 27:2490–2500. http://dx.doi.org/10.1002/jbmr.1706